Multiple load path damage detection with optical fiber Bragg grating sensors

CUSTOMER: European Commission

NLR – Royal Netherlands Aerospace Centre

Multiple load path damage detection with optical fiber Bragg grating sensors

Problem area

Many (aircraft) structures have multiple load paths where after a (partial) failure of a load path the remaining structure can carry the limit load without catastrophic failure or too severe impact on the operational characteristics of the whole structure, until the structure is repaired, replaced or modified. In this paper a new damage indicator for structural health monitoring is presented that can detect a (partial) load path failure for a multiple load path structure, based on variable amplitude strain response measurements by fibre-optic Bragg grating sensors. This fibre optic sensor is one of the most promising strain sensors for this purpose because it: is light weight, is tolerant for harsh environments (temperature, chemical components), has long term stability and durability, is completely passive and has no interference with other signals.

Description of work

The damage indicator is defined as a ratio of the strain response summation of the current strain time variation measured at all FBG sensors and a reference strain time variation measured at the same FBGs. For application in real structures with varying loads and environmental conditions, it is insensitive for the load time variation as well as temperature. The FBG strain response due to a load variation can be easily computed by means of a finite element analyses. In this way, an optimal number, location and orientation of strain sensors can be derived for complex structures.

A test was performed on a box-shaped structure representative of a typical aircraft structure to validate the damage indicator, demonstrating that the damage indicator is able to detect a damaged load path at an early stage of failure with few sensors per load path. From finite element analyses, the damage size can even be determined from the damage indicator value for a known damage scenario, making it a level 3 SHM system.

Results and conclusions

From the simulation and test, it can be concluded that the damage indicator is able to detect a damaged load path at an early stage of failure. It suffices to monitor each load path by only one strain sensor, although with more sensors damage may be detected in an even earlier stage. The damage size can be determined from the damage indicator value for a known damage scenario (as applied in the damage tolerance analysis), from finite element analyses, making it a level 3 SHM system. The presented damage indicator is not sensitive for temperature effects and therefore the SHM system does not require additional temperature sensors. Also, the damage indicator is not sensitive for the applied load time variation, making it robust, and it can be computed on a flight-by-flight basis, drastically reducing the inspection interval. Moreover, it can distinguish a debonded sensor from a load path failure and a broken fibre or sensor can easily be detected by the sensor system, preventing falls calls.

Applicability

The new damage indicator can be used in for structural health monitoring applications of multiple load path structures like the wing structure consisting of multiple spars and a lower and upper skin that often can sustain a broken spar, the vertical stabilizer and wing attach fittings, a wing carry through bulkhead or engine mounts.

GENERAL NOTE

This report is based on an article published in Structural Health Monitoring journal, 2020, by SAGE.

Multiple load path damage detection with optical fiber Bragg grating sensors

AUTHOR(S):

F.P. Grooteman   NLR

NLR – Royal Netherlands Aerospace Centre

CUSTOMER	European Commission
CONTRACT NUMBER	EU CS2 grant agreement no. 685704
OWNER	Netherlands Aerospace Centre (NLR)
DIVISION NLR	Aerospace Vehicles
DISTRIBUTION	Unlimited
CLASSIFICATION OF TITLE	UNCLASSIFIED

APPROVED BY:		Date
AUTHOR	F.P. Grooteman	16-11-2020
REVIEWER	M.J. Bos	16-11-2020
MANAGING DEPARTMENT	M.J. Bos	16-11-2020

Summary

In this paper a new damage indicator is presented that can detect a (partial) load path failure for a multiple load path structure, based on variable amplitude strain response measurements by fibre-optic Bragg grating sensors. Many (aircraft) structures have multiple load paths where after a (partial) failure of a load path the remaining structure can carry the limit load without catastrophic failure or too severe impact on the operational characteristics of the whole structure, until the structure is repaired, replaced or modified.

The damage indicator is defined as a ratio of the strain response summation of the current strain time variation measured at all FBG sensors and a reference strain time variation measured at the same FBGs. For application in real structures with varying loads and environmental conditions, it should be insensitive for the load time variation as well as temperature. The FBG strain response due to a load variation can be easily computed by means of a finite element analyses. In this way, an optimal number, location and orientation of strain sensors can be derived for complex structures. A validation test was performed on a box-shaped structure representative of a typical aircraft structure to validate the damage indicator, showing that the damage indicator is able to detect a damaged load path at an early stage of failure with few sensors per load path. From finite element analyses, the damage size can even be determined from the damage indicator value for a known damage scenario, making it a level 3 SHM system.

Contents

Abbreviations

ACRONYM	DESCRIPTION
CTE	Coefficient of Thermal Expansion
CSI	Crack Severity Index
FBG	Fibre Bragg Grating
mu	Microstrain
NDI	Non-Destructive Inspection
nDI	(Normalised) Damage Indicator
RT	Room Temperature
S4R	Spectrum Strain Severity Summation
SG	Strain Gauge
SHM	Structure Health Monitoring
a_0	Initial crack size
a	Crack size
Δa_i	Crack extension
C, m	Crack growth material parameters
GF_0	Gauge factor at room temperature
ΔGF	Deviation in gauge factor per 100 degrees Celsius
K	Stress intensity factor
ΔK	Difference in stress intensity factor
N	Number of load cycles
p_e	Strain-optic coefficient
T	Temperature
α_Λ	Thermal expansion coefficient
α_n	Thermo-optic coefficient
β	Geometry factor
σ	Stress or standard deviation
λ_0	Nominal wavelength
μ	Mean value

1   Introduction

The airframe of civil aircraft is designed according to the damage tolerance philosophy [1]. The damage tolerance philosophy recognizes that damage can occur and develop during the service life of an aircraft. Also, it assumes that damages can be present in a pristine structure. Safety is obtained by the requirements that either: (1) any damage be detected by routine inspection before it results in a dangerous reduction of the static strength (inspectable components), or (2) initial damage shall not grow to a dangerous size during the service life (non-inspectable components). The damage tolerance philosophy distinguishes two concepts:

1. <u>Fail-safe concept</u> where the required residual strength of the remaining intact structure shall be maintained for a period of unrepaired usage through the use of multiple load paths or damage arrest features after a failure or partial failure. The period of unrepaired usage necessary to achieve fail-safety must be long enough to ensure the failure or partial failure will be detected and repaired prior to the failure of the remaining intact structure.
2. <u>Slow damage growth concept</u> where flaws, defects, or other damage are not allowed to attain the size required for unstable, rapid propagation failure. This concept must be used in single load path and non-fail-safe multiple load path structures. Significant growth resulting from manufacturing defects or from damage due to high-energy impact is not allowed for composite structures.

The shortcomings of the deterministic single load path slow crack growth concept are that it doesn't address the issues of continuing damage in the adjacent structure, safe periods of unrepaired usage after a load path failure and the fact that the fail-safety will be jeopardized later in life by the onset of widespread fatigue damage [2]. The fail-safe design [2] is the preferred concept since it provides large damage capability and is the only concept that protects against all forms of damage an aircraft may encounter during its lifetime. Damages can come from manufacturing induced damages like inclusions, scratches, improper bonding and in-service induced damages due to fatigue damage, environmental damage such as corrosion, or accidental damage due to overloads and discrete source damage such as bird strike, tool drop, ground service activities, engine bursts or even battle damage.

Many (aircraft) structures have multiple load paths where after a (partial) failure of a load path the remaining structure can carry the limit load without catastrophic failure or too severe impact on the operational characteristics of the whole structure, until the structure is repaired, replaced or modified. Examples are, the wing structure consisting of multiple spars and a lower and upper skin that often can sustain a broken spar, the vertical stabilizer and wing attach fittings, a wing carry through bulkhead or engine mounts. The (partial) failure shall be either readily detectable by visual inspections or through a malfunction event, for instance fuel leakage or loss of cabin pressure. However, also other inspections can be performed to detect any problem long before an expensive (partial) load path failure or in cases where a visual inspection cannot be performed. The main non-destructive inspection (NDI) methods employed in practice are visual, radiography, ultrasonic, eddy current, magnetic particle and dye penetrant methods. Visual inspection is the most common applied method for locating surface damage, although limited to relatively large anomalies and easy to access locations. The detectable damage size with a specific NDI method is the damage size that can be detected with a 90% chance and 95% confidence.

During the last decades, a lot of research has been dedicated to more automated systems like structure health monitoring (SHM), which consists of a network of sensors to detect changes in the dynamic response of a structure over time from data gathered at different states, an initial reference state considered as the undamaged state, and the current (damaged) state. From the sensor response data, damage indicators are derived that determine the presence (level 1), location (level 2), and if possible the severity (level 3) and type of the damage (level 4). Each level in

principle requires more sensors and may therefore be inappropriate from an economical perspective depending on the current inspection cost, repair/replacement costs and SHM system costs. A number of characteristics of an SHM system are: a reduction of the high manual inspection costs, detection of damage at non accessible locations and the inspection frequency of an automated SHM system will be much higher (each flight) than conventional NDI methods (years). Some challenges are: the costs of the SHM system, demonstration of the system's reliability, certification, self-diagnostics of the system (e.g. to detect a sensor failure) and repair of the system (e.g. in case of a broken sensor).

The main objectives of SHM are to reduce the cost of ownership and to improve the system operational availability. Application of a reliable SHM system for multiple load path (fail-safe) structures to detect (partial) failure of a load path(s) is an interesting application area. This would prevent periodic (costly) inspections and allows maintenance on demand after the system detects a (partial) failure. Especially in difficult to inspect areas, for example the spars in a wing or tail or the interface of the wing and tail to the fuselage, this could yield a significant reduction in maintenance costs. The SHM system has a much higher inspection frequency that even would allow a redesign of the structure, because damage will be detected much earlier. This also has the potential to result in lighter/cheaper structural designs.

Various types of sensors exist to monitor the condition of the structure and to signal in time that damage is present, such as acoustic and ultra-sonic sensors [3]. These operate in the mid (kHz to MHz) to high frequency range (MHz and beyond). A sensor that can also operate in the low frequency range is the optical fibre Bragg grating (FBG). An FBG is a small segment in an optical fibre in which a periodic variation of the refractive index is inscribed by an ultraviolet laser. The segment reflects particular wavelengths of the light and transmits all others. Stretching or compressing the fibre causes a shift of the reflected wavelength which can be correlated with a strain value by means of calibration [4]. Optical sensing based on FBGs has a number of appealing advantages for application in (aircraft) structures, such as light weight, multiple sensors in one fibre, tolerant for harsh environments (temperature, chemical components), long term stability and durable, completely passive and no interference with other signals. The optical fibres can be embedded in the (composite) structure or surface mounted. The latter has the big advantage that a sensor can be installed any time during manufacturing and operational life and a broken fibre can be repaired or replaced. Various commercial interrogators exist, like the Gator from Technobis [5] applied in this research. The interrogators currently in use can operate in the frequency range up to MHz range, for instance the SuperGator currently under development at Technobis or Optics11 [6] allowing for acoustic emission measurements with FBGs.

FBG strain sensors have been applied in many applications, such as load monitoring [7], impact localization in composite structures [8] and damage detection. For damage detection various damage indicators have been developed for composite as well as metallic structures often comparing the structural response of the current state against a reference state. Many papers have been published that use the change in vibration response of a structure, [9] and [10] provide an excellent review. These normally are based on lower frequency modes (<2 kHz) and can only detect larger damages that significantly reduce the stiffness of the structure. Due to the recent availability of commercial high sample speed interrogators, more and more research is conducted towards damage detection by means of acoustic emission [11]-[12], utilizing higher-frequency modes (<500 kHz), which is a promising technology for FBGs to detect smaller damages than possible with a vibration-based approach.

In many structures, like aircraft, the strain response in the structure during operation is often dominated by a low frequency (< 100 Hz) alternating load. A vibration-based or acoustic emission damage identification will therefore not apply during operation. In this paper, a damage identification method is introduced that is based on low frequency strain response due to an alternating external load with variable amplitude to detect a growing damage, applied to a multiple load path structure.

2 Damage index

The objective is to detect a (partial) load path failure in a multiple load path (fail-safe) structure by measuring the strain in each load path at one or a few (most) critical locations. In an aircraft the strain response at any location shows a variation over time due to changes in (variable amplitude) load caused by the different flight stages (ground, climb, cruise, and descent), gust and manoeuvres. Moreover, the temperature significantly varies during a flight (from ground temperature as high up to 85 to about -50 °C in flight and back) causing additional fluctuations in strain level. A suitable damage indicator therefore should be able to transform the variability in strain into a single indicator that signals for damage in one or more load paths. The strain fluctuations due to temperature changes can be corrected for but requires additional sensors that measure the local temperature. Therefore, ideally no temperature correction should be necessary.

A very promising damage indicator (DI) is based on the crack severity index (CSI), [13] and [14], as a relatively simple means to determine the effect of changes in operational usage on damage growth using only the measured strain sequence. The DI is derived from a simple damage growth model. Here a crack growth model is applied applicable for metallic structures, but this is applicable to damage growth in composite structures as well [15]. The growth of a crack (damage accumulation) due to an alternating variable amplitude load time variation is a summation of the crack growth in each individual load cycle of the time variation:

$$a_n = a_0 + \sum_{i=1}^{N} \Delta a_i \tag{1}$$

where a_0 is the initial crack size, N the number of load cycles in the time variation and Δa_i the crack extension in the ith cycle. The crack extension per cycle can be obtained from a crack growth equation. The simplest one is the Paris type equation:

$$\Delta a_i = C \Delta K_i^m \tag{2}$$

where C and m are material parameters fitted from experimental crack growth data obtained from coupon tests made of the same material and of similar thickness; ΔK is the difference in stress intensity factor between the minimum and maximum stress level in the cycle:

$$\Delta K_i = K_{max,i} - K_{min,i} \tag{3}$$

The stress intensity factor K reflects the stress distribution around the crack tip and as such can be correlated with crack extension. It depends on the geometry of the feature in which the crack grows, expressed in terms of a dimensionless β-factor, the applied remote stress σ and the length of the crack a:

$$K = \beta(a)\sigma\sqrt{\pi a} \tag{4}$$

Substituted in the previous equation yields:

$$\Delta K_i = \beta(a)\left(\sigma_{max,i} - \sigma_{min,i}\right)\sqrt{\pi a} \tag{5}$$

For many simple geometries and simple load cases the geometry factor β can be obtained from handbooks [16]. For more complicated geometries or load cases the stress intensity factor solution can be computed by means of finite element analyses.

Combining the above equations gives:

$$\frac{\Delta a_i}{\left(\beta(a)\sqrt{\pi a}\right)^m} = C\left(\sigma_{max,i} - \sigma_{min,i}\right)^m = D\left(\varepsilon_{max,i} - \varepsilon_{min,i}\right)^m \tag{6}$$

The left-hand-side only contains crack geometry (damage) dependent terms being a measure for the damage and the right-hand-side only contains stress (σ) or strain (ε) cycle dependent terms and as such is a measure for the severity of the time variation. Two different spectra yielding the same value for the right-hand-side term will cause a similar crack extension. The right-hand-side-term is approximated by a cycle-by-cycle summation over the whole time variation:

$$S4R = D \sum_{i=1}^{N} (\varepsilon_{max,i} - \varepsilon_{min,i})^m \tag{7}$$

This term is called the Spectrum Strain Severity Summation (referred to as S4R).

The damage index is now defined as a ratio between the S4R value of the current strain time variation measured at an FBG sensor and a reference strain time variation measured at the same FBG.

$$DI = \frac{S4R}{S4R^{ref}} \frac{N^{ref}}{N} = \frac{\sum_i (\varepsilon_{max,i} - \varepsilon_{min})^m}{\sum_i (\varepsilon_{max,i}^{ref} - \varepsilon_{min}^{ref})^m} \frac{N^{ref}}{N} \tag{8}$$

Different spectra can have different number of cycles, therefore both terms in the above equation are normalized with the number of cycles in the time variation. Note that the material parameter *D* is divided out of the expression. The parameter *m* is a material constant, having a value close to *m*=3 for aircraft structure metals. Since the damage index is a ratio and the parameter *m* appears in both the nominator and denominator, it is not very sensitive for the chosen value.

By means of this equation, two measured variable amplitude strain spectra for the same FBG, a reference and the current time variation, can be transformed into a single valued damage indicator, where the length of both spectra may vary. The reference (undamaged) strain time variation can be obtained from the measurement performed at the start of the usage period or any of the measurements performed thereafter. The latter may be required in case of modifications/repairs after which a new reference may be needed.

For each of the FBG sensors, installed in different load paths, the *DI* is computed after each flight. A further normalization of the damage index can be obtained by subtracting the mean damage indicator obtained for all sensors and subdividing by its variance, similar as applied to transform a normal to a standard normal distribution:

$$nDI_{FBGi} = \frac{DI_{FBGi} - \mu_{DI}}{\sigma_{DI}} = \frac{DI_{FBGi} - \mu_{DI}}{0.1\,\mu_{DI}} > DI_{threshold} \tag{9}$$

The normalized damage index *nDI* value represents the number of standard deviations away from the zero-mean. For values above some threshold value $DI_{theshold}$, this provides an indication of the presence of damage. If a damage is present in one or more of the load paths, the strain in this load path will decrease and load will be transferred to neighbouring load paths. This will cause a negative damage index value for the damaged load path and a positive damage index value for the neighbouring load path(s). For a fully broken load path, the strain response will be near zero, as well as *DI*. The normalized damage index *nDI* then becomes -μ_{DI}/σ_{DI}. By selecting a fixed value for σ_{DI} equal to 0.1xμ_{DI}, instead of a computed value from the DI_{FBGi}, the *nDI* value indicating full load path failure always becomes -10, which is more consistent for an operator. In section 4 it will be demonstrated that the damage index is not sensitive for temperature and load time variation length.

3   Numerical simulations

The damage indicator, based on strain response at the start and end of a series of load cycles, can easily be simulated by means of static linear finite element analyses. In this way, an optimal number, location and orientation of strain sensors can be derived for complex structures. Moreover, the robustness and reliability of the SHM system, e.g. broken or disbonded sensor(s) and variation in damage scenarios, can be largely assessed by simulation instead of expensive testing. The deterministic finite element analysis can even be combined with a generic probabilistic analysis tool to examine the influence of other sources of uncertainty, like material variability. Only a limited amount of testing to validate the results from the numerical analyses is required, which is a huge advantage over other sensor types which are (much) more difficult to simulate, like piezoelectric sensors.

The selection of the sensor locations is demonstrated here for a box-shaped structure consisting of two similar aluminium (7075-T6) panels (400x820x2 mm) with 3 stiffeners each at a distance of 90 mm depicted in Figure 1 and Figure 4. Four slots (175x25 mm) were inserted in the upper half of each panel in between the stiffeners to create three, more individual, load paths. The structure has various similarities with a vertical tail plane or wing structure.
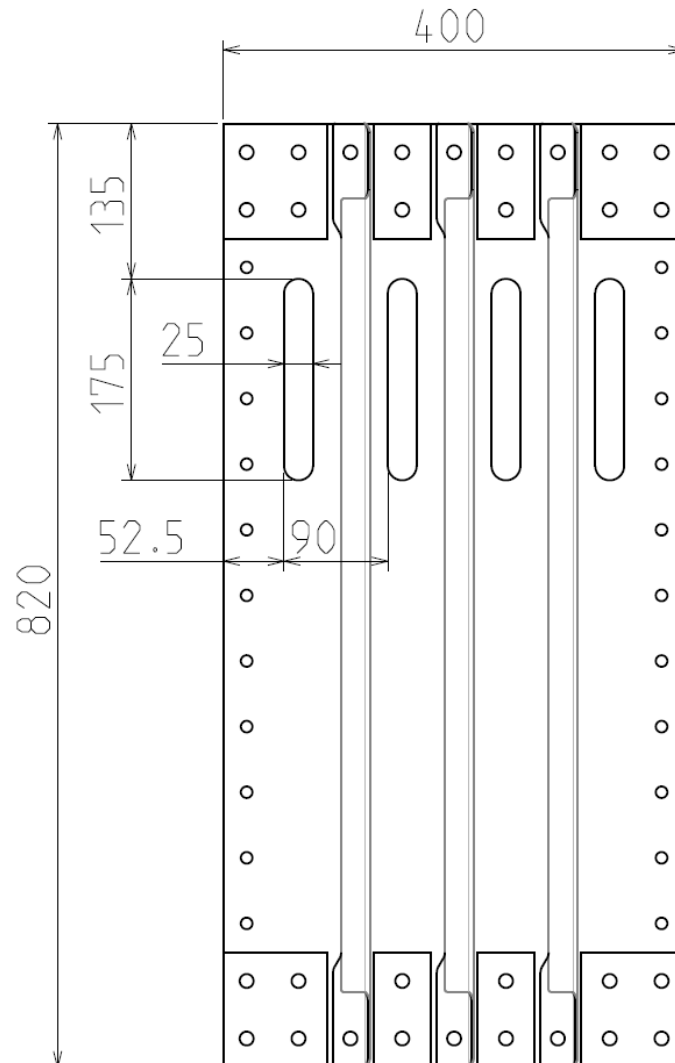

Figure 1: Stiffened aluminium panel

A possible damage scenario is that of a crack in the skin on one side of the centre stiffener that grows due to alternating loads towards the stiffener. As a result of some load redistribution to the stiffener and the intact skin on the other side of the stiffener, the crack growth will slow down when it approaches the stiffener. Due to the increased load in the intact skin, a new crack can more easily start at the other side of the stiffener and also grows towards the stiffener. Both cracks now keep growing until also the skin under the stiffener is fully cracked. Due to the increased load transfer to the stiffener a crack will start growing in here as well until it finally results in a broken stiffener and fully broken load path. Other scenarios are possible and can be analysed in the same way as demonstrated herein.

A finite element model of the box-shaped structure was created in Abaqus to determine the number and positions of the FBG sensors. The finite element model consisted of 100544 nodes and 92546 linear elements and an artificial through crack was modelled half-way the width of the middle slot, as indicated in Figure 2. Here the best FBG orientation, in load direction, is obvious but this is more complicated for complex structures in geometry and loading and can be obtained from the finite element analysis as well. With the finite element model, strain fields for a unit load were computed for the undamaged panel and subsequently used to compute the strain variation over time for the given load time history, for the following four intermediate damage states, depicted in Figure 2:

1. Skin failure right of the centre stiffener (crack size 25 mm)

2. Skin failure left and right of the centre stiffener (crack size 25 + 32.5 mm)

3. Full skin failure under the centre stiffener (crack size 65 mm)

4. Fully broken centre stiffener, i.e. full load path failure (crack size 90 mm)

Figure 2 shows the obtained strain distribution in load direction for the four damage states, from which optimal strain sensor locations can be selected. One strain sensor was selected in load direction on both sides of each stiffener, 40 mm from the bottom end of the slot, see Figure 5. Additionally, one strain sensor was installed on the web of the centre stiffener. On the second undamaged panel only one strain sensor was selected on the right side of each stiffener, see Figure 6.
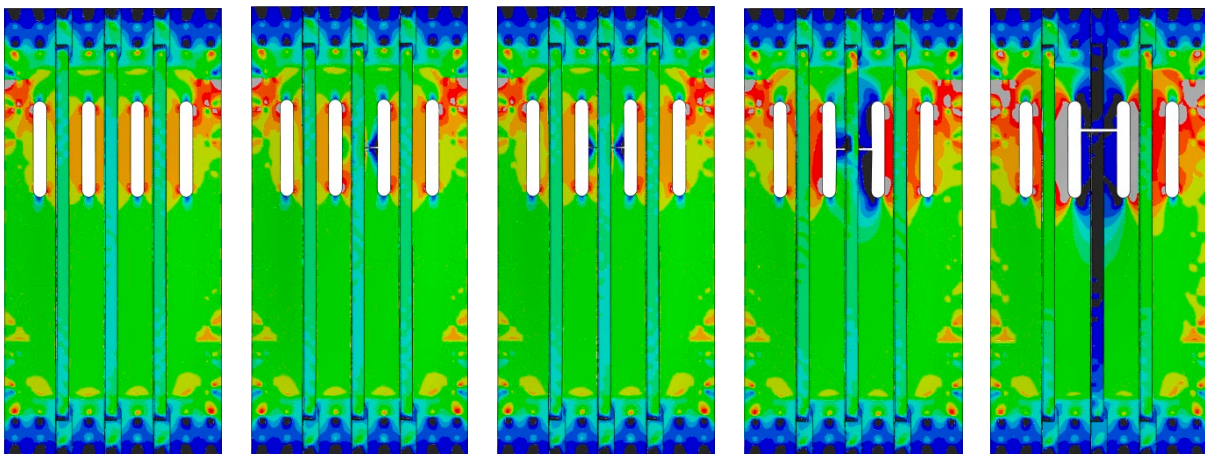

Figure 2: Strain field in load direction for the undamaged panel (left) and subsequent four damage states

From the computed strain fields, the unit load strains at the different strain locations were derived and multiplied with the actual time variation, representing the simulated local stress spectra at each location. Subsequently, these spectra were used to compute the normalized damage indicator *nDI* for each damage state, depicted in Figure 3. The sensors on the front panel (with damaged centre stiffener) are labelled S1 to S8 (note that S2 is missing to obtain the same labels as applied in the test) and on the rear panel S9 to S11. The value of *nDI* should be around zero when no

damage is present. This clearly is the case for the undamaged load paths in the rear panel monitored by S9, S10 and S11 (blue dashed lines) for all four damage states of the front panel. Also, for the first smallest damage state most strain sensors on the front panel show a *nDI* value around zero. The strain sensors in the damaged load path (S5 and S6) have a negative *nDI* value when the strain in this load path decreases due to an increasing damage. The sensors closest to the damaged load path (S4 and S7) show a strong increase in *nDI* due to a strain increase caused by load redistribution from the nearby damaged load path. An upper and lower threshold level of ±2.0 standard deviations is set below or above which the normalized damage indicator convincingly indicates that damage is present. A standard deviation of ±2 sigma away from the mean of the normalized damage indicator (eq 9) indicates a high probability of the presence of damage due to a significant loss of stiffness, to avoid falls calls and also to cope with (load or environmental) uncertainties in a real application, for instance noise.

At the first damage state, the damage index for S5 is already below threshold, because the strain level significantly drops at this damaged side of the stiffener. Some load is transferred to the skin on the other undamaged side causing some increase in the strain and damage index for S6 as well. At damage state 2, with a skin crack at both sides of the stringer, the strain in this load path decreases and both S5 and S6 yield a negative normalized damage index *nDI* at or below threshold indicating the damage. The strain and therefore *nDI* at S3, S4, S7 and S8 in the neighbouring load paths and S1 on the web of the centre stringer slightly increases due to some load transfer and yield a *nDI* around 1 not signalling the damage. At damage state 3, full skin failure, the strain and *nDI* at the sensors in the damaged load path (S5 and S6) further decreases and vice-verse increases in the neighbouring load paths (S4 and S7). At damage state 4, full load path failure, the *nDI* for S5 and S6 is -10, indicating full load path failure. The *nDI* for S4 and S7 has further increased.

In conclusion, from damage state 2, the damaged load path can correctly be identified by the sensor(s) in the load path, as well as from damage state 3 by the sensors in the neighbouring load paths, long before actual full load path failure. It should be noted that it takes a considerable amount of time (flights) to grow the damage from one state to the other, in which period there are many SHM inspection moments to detect the damage. From the finite element analyses, the damage size can be obtained for the *nDI* value for each of the sensors, i.e. each point in Figure 3, arriving at a level 3 SHM system. It suffices to have one sensor per load path, e.g. S3, S5, S7 or S4, S6, S8.
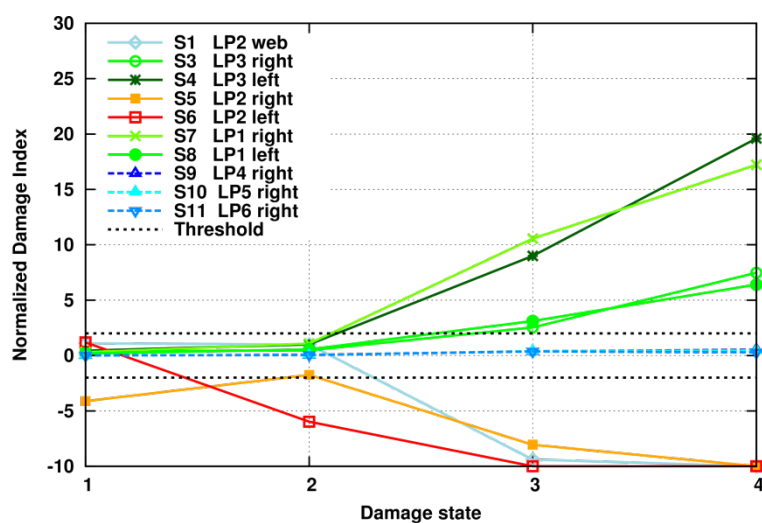

Figure 3: Normalized damage index versus the damage state obtained from FEM

4   Experimental results

A test was performed on the box-shaped structure analysed in the previous section. The component is mounted in a generic SHM test rig developed at NLR for verification and validation of SHM sensor networks and algorithms for complex components. Components can be installed in the rig by means of a modular interface. The rig can apply bi-axial loads by means of two actuators up to a frequency of around 20 Hz. Also, it is possible to add a shaker to apply additional dynamic loading up to a few kHz. A climate chamber can be installed to run tests at elevated or low temperatures in the typical temperature range of aerospace components, -50 to 85 °C. Figure 4 shows part of the SHM test rig (in blue) with the double stiffened panel mounted inside the opened climate chamber. The small red box visible on top of the two metal beams in front of the panel is the commercially available optical chip based fibre optic interrogator system (Gator) manufactured by Technobis [5]. The Gator system has one input channel for fibre with 8 FBGs and has a wavelength range of [1514, 1586] nm with a maximum sample rate of 19.23 kHz and an achieved measurement accuracy of 1 microstrain.

Figure 4: SHM test bench at NLR with mounted double stiffened aluminium panel in climate chamber with the fibre optic interrogator (Gator, small red box) from Technobis

Several FBG sensors were installed on the rear side of the front panel, using the adhesive M-Bond 200 to adhere the FBG to the panel and the adhesive HBM X60 to cover the FBG to achieve a stiff bond. Both are well-known for adhering strain gauges to surfaces a well. An FBG was installed on both sides of each stiffener, see FBG3 to FBG8 in Figure 5. Furthermore, one FBG (FBG1) was installed on the web of the centre stiffener and one (FBG2) on a small aluminium rectangular sheet to act as a temperature sensor, visible in the top of Figure 5. This small rectangular sheet was made of the same material as the panel and was mounted to the rear of the front panel by means of some silicon to allow free expansion/compression of the sheet during temperature fluctuations. The surplus optical fibre in between any two FBG locations was coiled up with a sufficiently large radius to prevent optical losses and was attached to the panel with some silicon to prevent breakage of the fibre. On both sides of the fibre a connector was installed to be able to access all FBGs in case of fibre breakage.

For several FBG locations, also a quarter bridge strain gauge and a PT100 temperature sensor were installed next to the FBG, see Figure 5. The strain gauges were installed for comparison of the FBG strain responses. The PT100 sensors were used to monitor the temperature of the panel at a number of locations during cooling down and heating up of the panel and to compare against the FBG temperature sensor. On the rear panel, only a single strain gauge was installed in each of the load paths, see Figure 6. An overview of all installed sensors and their position is given in Table 1.
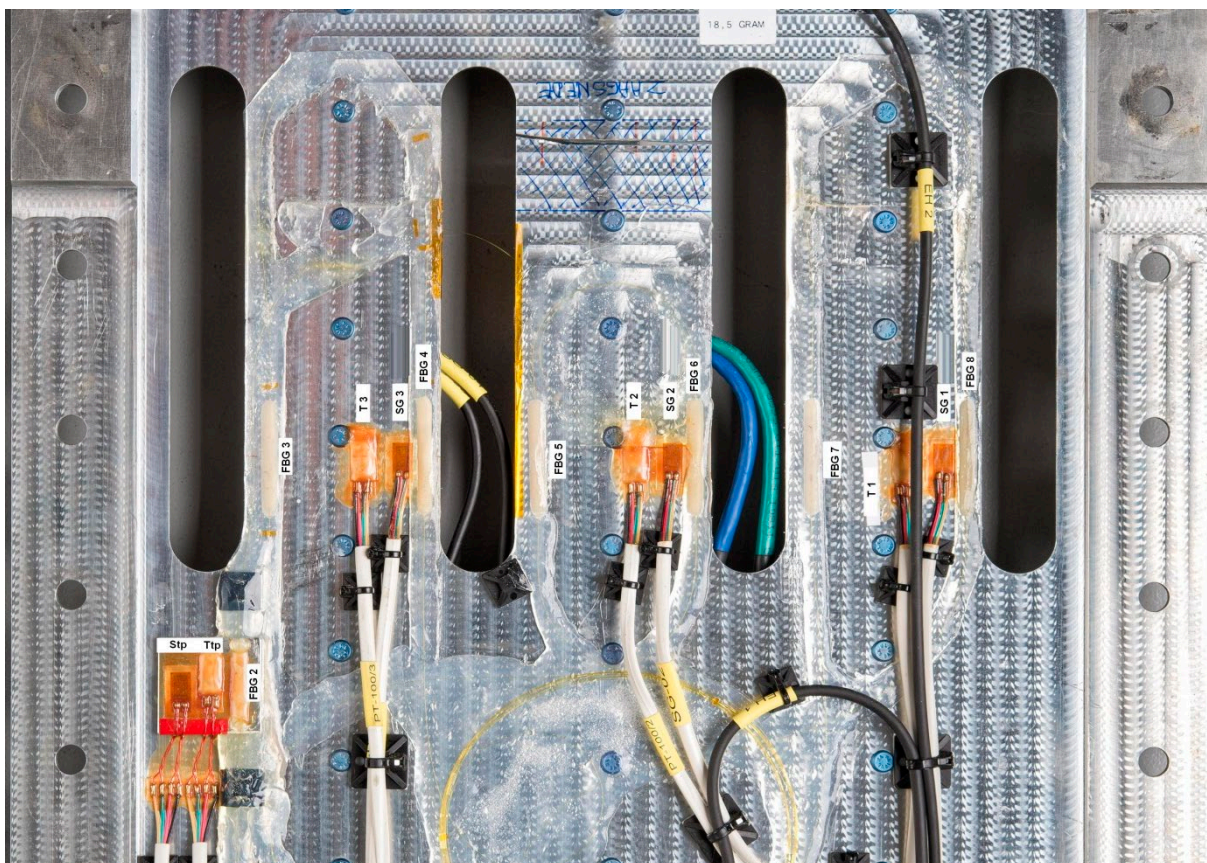

Figure 5: Installed FBG, strain gauge and temperature sensors on the rear side of the front panel

Figure 6: Installed strain gauges and temperature sensors on the rear panel

Table 1: Schematic sensor labels per load path, located left, on or right of the stiffener

Front panel							
Load path 1		**Load path 2**			**Load path 3**		**Sheet**
Left	**Right**	**Left**	**On**	**Right**	**Left**	**Right**	
FBG8	FBG7	FBG6	FBG1	FBG5	FBG4	FBG3	FBG2
SG1		SG2	SG4		SG3		Stp
T1		T2	T4		T3		Ttp
Rear panel							
Load path 4		**Load path 5**			**Load path 6**		
Left	**Right**	**Left**		**Right**	**Left**	**Right**	
	SG9					SG11	
	T9			SG10		T11	

Airbus supplied a typical (wing) variable amplitude load time variation consisting of various flights of which 90 were applied in the test. In Figure 7, a detail of the scaled time variation for three flights as applied in the test is depicted, clearly showing a taxiing, climb, cruise and descend phase. The time variation was scaled for the test article, yielding a maximum actuator load of 100 kN. With this time variation, low cycle dynamic tests were performed for the undamaged and four damaged states, described in section 3 and depicted in Figure 8, at room temperature (around 18 °C) and at -30 °C. During each test, the load time variation was applied at a rate of 13 Hz and the load, temperature, FBG and strain gauge responses were measured and stored in a database. For each five (undamaged and

damaged) panel configurations, first the test at room temperature was performed after which the climate chamber was closed and the panel was cooled down to -30 °C. The panel was cooled by spraying nitrogen inside the climate chamber through a number of nozzles. Temperature sensors were used to control the start and stop of the nitrogen flow, causing the oscillations in the temperature sensor profiles during cooling down, as depicted in Figure 9. After approximately one hour a stable situation was obtained and the load time variation was applied. After this test, the climate chamber was opened on the front and side, and the panel warmed up to room temperature overnight.
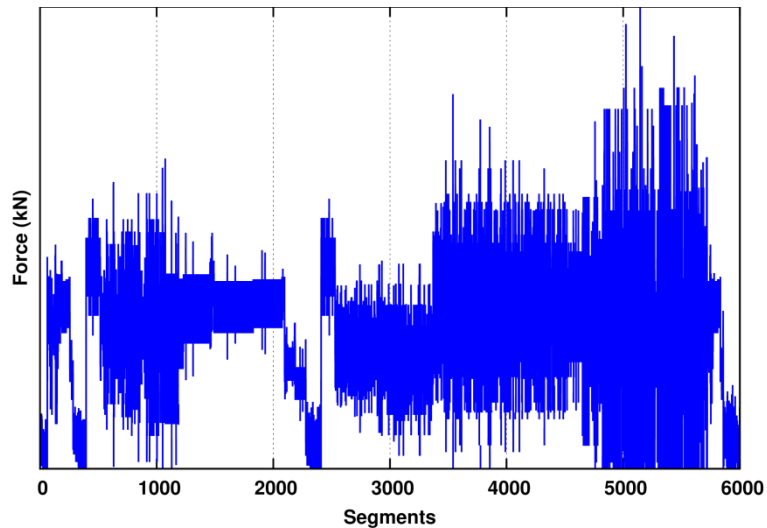
Figure 7: Detail of applied load time variation for three individual flights

Figure 8: Artificial damage states in front panel centre load path, from top left (crack right of stringer) to bottom right (fully failed load path), see also Figure 2
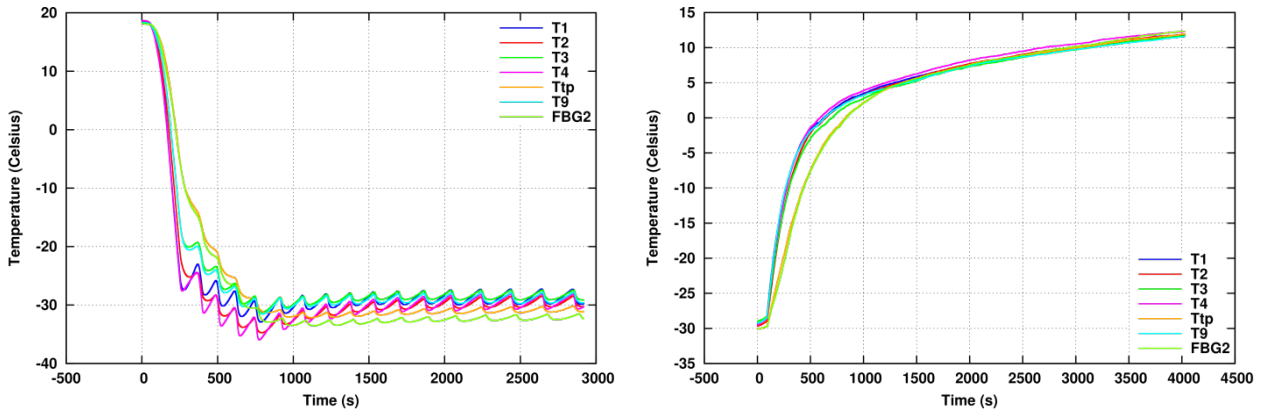
Figure 9: Measured temperature profiles during cooling-down (left) and warming-up (right) phase of the test article

Figure 10 shows the measured strain response in microstrain (mu) for a few load cycles for two FBG/SG pairs (see also Figure 5 and Table 1) at room temperature. Both sensor types give a similar strain response. Small differences are due to the slight difference in sensor location. The FBG sensor/interrogator combination had a much (five times) lower noise level, as can be noted in Figure 10. Hence, more accurate measurements could be obtained with the FBGs.
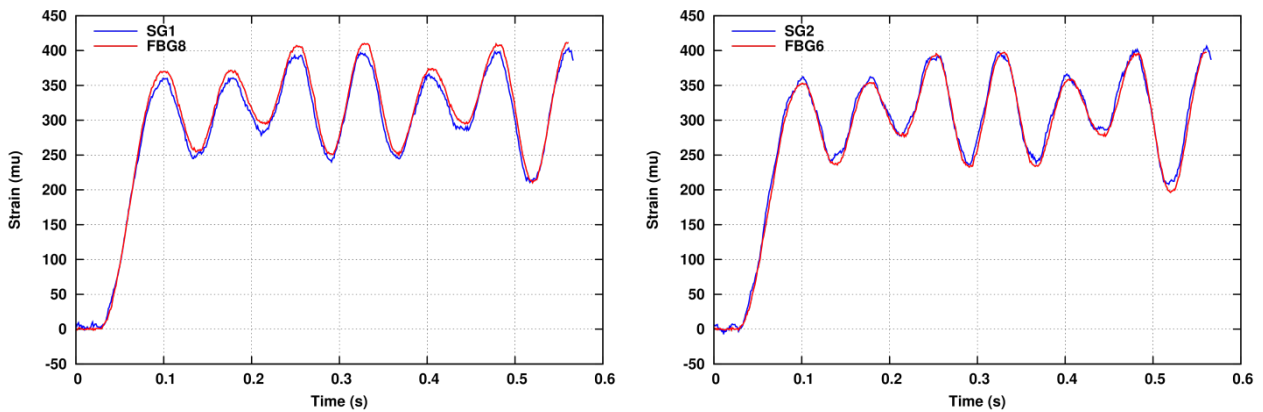

Figure 10: Comparison of strain responses for two FBG and strain gauge pairs for a number of load cycles

The normalized damage index *nDI* (9) was computed for each damage state from the measured variable amplitude strain responses at each strain sensor, in which the reference time variation was obtained on the undamaged panel. The mean value μ_{DI} was the average of the non-normalized damage indicators *DI* of all sensors. As explained in section 2, for the standard deviation σ_{DI} a fixed value of $0.1 \times \mu_{DI}$ is applied, yielding a fixed lower damage indicator value of -10 that signals full load path failure (no load transfer) at the corresponding sensor.
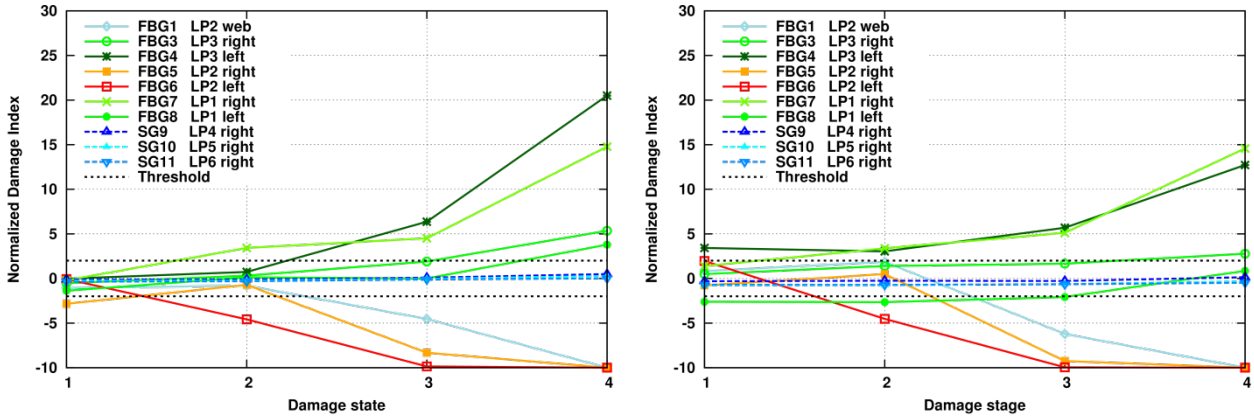
Figure 11: Normalized damage index versus the damage state from measurements at RT (left) and -30 ℃ (right), generated from the first 5 flights of the reference time variation and only the 21st flight of the damaged spectra

Figure 11 depicts the change in damage index as function of the damage states. On the left the results are presented for the measurements at room temperature and on the right at -30 °C, which are similar as the results obtained with the numerical simulation depicted in Figure 3, having an error between the numerical and experimental values as a percentage of the full scale of less than 10% for room temperature and 20% for -30 °C. The value of the damage indicator is around zero when no damage is present. This clearly is the case for the undamaged load paths in the rear panel monitored by SG9, SG10 and SG11 (blue dashed lines) for all four damage states in the front panel, and also for most strain sensors on the front panel for the first smallest damage state. The sensors in the damaged load path (FBG5 and FBG6) have a negative normalized damage index value when the strain in this load path decreases due to an increasing damage, and the sensors closest to the damaged load path (FBG4 and FBG7) show a positive normalized damage index due to a strain increase caused by load redistribution from the damaged load path. The dotted black-lines in the plots represent the damage indicator threshold value ($\pm 2.0\sigma$) below which no definitive conclusion can be drawn about any damage present, due to small fluctuations in the damage index caused by for instance noise. The damage and its location (level 2) is correctly signalled at damage state 2, long before actual full load path failure, see section 3 for a more detailed discussion. The damage index value depends on the strain levels at the various sensors which on turn depend on a nearby crack size. The normalized damage index values in Figure 3 and Figure 11 can thus be correlated with a damage size for the structure at hand using FE simulations, making it even a level 3 SHM system.

Ideally, the damage indicator should be temperature independent, avoiding the need for temperature sensors, e.g. PT100 or additional FBGs. The relationship between FBG wavelength λ, strain ε and temperature T is given by:

$$\varepsilon = \frac{1}{(1 - p_e)} \left[\frac{\Delta \lambda}{\lambda_0} + (\alpha_\Lambda - \alpha_n)\Delta T \right] \tag{10}$$

in which λ_0 is the nominal wavelength after FBG installation on the structure, p_e the strain-optic coefficient (0.22 for a glass fibre), α_Λ the thermal expansion coefficient and α_n the thermo-optic coefficient. These values are strongly influenced by the material on which the FBG is installed. A value of 21.0 microstrain was selected for α_Λ - α_n that caused the temperature profiles for the FBG2 and Ttp sensors, measured on the small rectangular sheet, to coincide during warming up of the test article after a test at -30° Celsius, see Figure 9, which is close to the coefficient of thermal expansion (CTE) value of the aluminium sheet.

For strain gauges the relationship between strain and temperature is given by:

$$\varepsilon = (\varepsilon_T - C_0 - C_1 T - C_2 T^2 - C_3 T^3 - C_4 T^4)\frac{2}{GF}$$
$$GF = GF_0 \left(1 + \frac{\Delta T \, \Delta GF(\%)}{100 * 100}\right) \tag{11}$$

The measured strain at temperature T (ε_T) is corrected for temperature by the polynomial term of which the value for the coefficients C_i can be found on the strain gauge package. The second term corrects the gauge factor for temperature changes, in which GF_0 is the gauge factor at room temperature and ΔGF the deviation in gauge factor per 100 degrees Celsius that both can be found on the strain gauge package as well.

Figure 12 depicts the strain responses during the cooling-down phase for an FBG sensor. The plots depict the temperature corrected as well as the uncorrected strain response. The uncorrected FBG strains have an offset of approximately 1300 microstrain ($\alpha\Delta T/(1-p_e) = 21 \times (18+30)/0.78 = 1300$) and are very sensitive for temperature fluctuations (27 microstrain per degree Celsius). However, the FBG temperature correction, given by equation (10), is a linear relation while for a strain gauge this is a non-linear relation, given by equation (11). The damage indicator is based on a relative strain difference for each load cycle and therefore does not require a temperature correction in case of FBGs since the strain difference between any two successive load levels is independent on temperature, assuming the temperature is constant between two successive load levels, i.e. the load variation (typically larger than 1 Hz) has a much higher rate than the temperature variation being much more gradual. In case the temperature shows a significant temperature gradient over the structure, this still has no influence on the relative strain at the FBG location in a cycle. In case of strain gauges, a temperature correction is required and therefore temperature sensors, increasing the complexity of the SHM system.

The right plot in Figure 11, shows the normalized damage index obtained from the measurements at -30 °C using the FBG data not corrected for temperature, showing that the damage indicator works well for temperature uncorrected data. Some small differences can be observed, but these do not influence the correct indication of presence of damage.
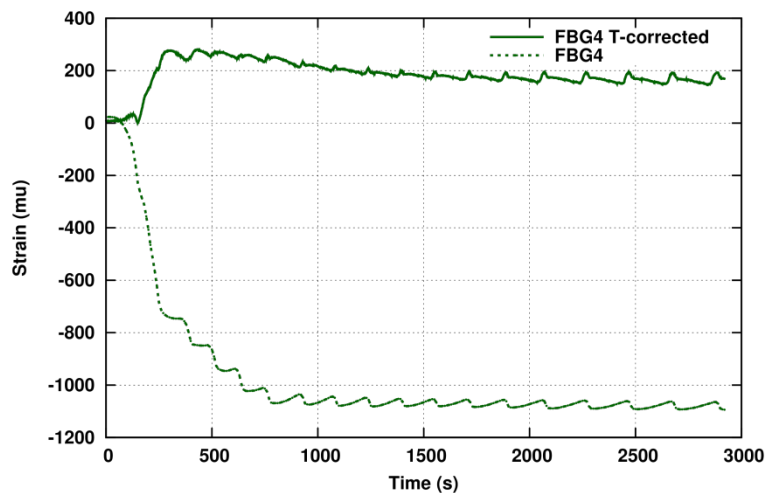

Figure 12: Temperature corrected (solid) and uncorrected (dashed) FBG strain responses during cooling down phase of the test article

Ideally, also the damage indicator should only require the data gathered during the next flight, to be able to monitor the damage on a flight-by-flight basis. To demonstrate this, the damage indicator was computed for various numbers of flights. The damage indicator curves in Figure 11 were generated from the first 5 flights of the measured reference time variation (undamaged state) and only the 21st flight of the spectra measured on the damaged states. Figure 13 shows the plots based on the first ten flights of the reference time variation and flights 81 to 90 for the damaged states. Other combinations using more flights for both the reference and damaged spectra, were examined as well yielding similar plots, not shown in here for reasons of space. This demonstrates that after a few number of flights

from the start of the usage period (reference set), the damage indicators can be determined for each successive flight. After a structural repair or modification in the region of interest, a new set of reference flights should be build consisting of the response measured during the first few flights after a repair or modification.

A broken fibre optic cable or defect FBG sensor can be detected by the interrogator system. A disbonded sensor, measuring no strain variation, will result in a high negative value indicating a failed load path but without an increase in the damage indicators of nearby sensors due to load transfer. A sensor disbond can therefore be distinguished from a damaged load path.
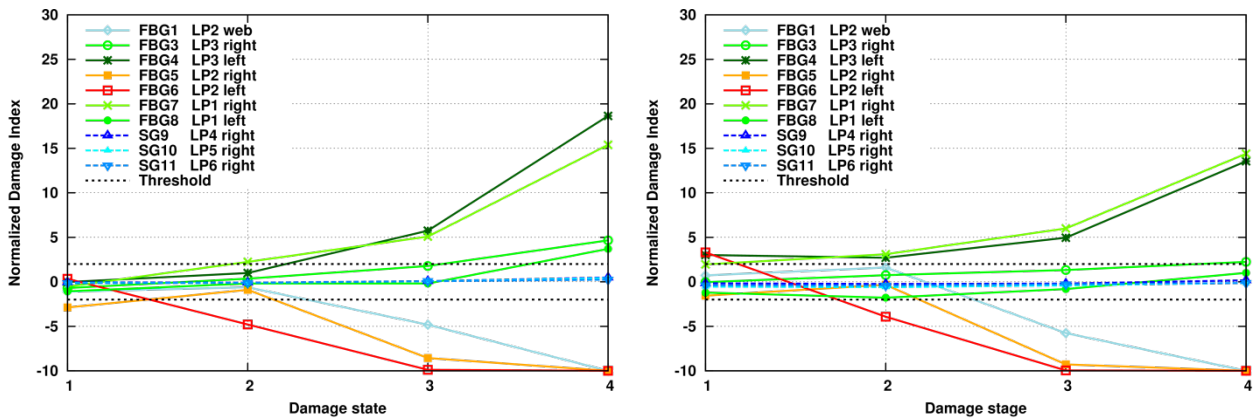

Figure 13: Normalized damage index versus the damage state from measurements at RT (left) and -30 ℃ (right), generated from the first ten flights of the reference time variation and flights 81 to 90 of the damaged spectra

5   Conclusions

In this paper a new damage indicator is presented that can detect a (partial) load path failure for a multiple load path structure, based on strain response measurements. The most promising strain sensor for this purpose is a fibre optic FBG sensor because it: is light weight, is tolerant for harsh environments (temperature, chemical components), has long term stability and durability, is completely passive and has no interference with other signals. From the simulation and test, it can be concluded that the damage indicator is able to detect a damaged load path at an early stage of failure. It suffices to monitor each load path by only one strain sensor, although with more sensors damage may be detected in an even earlier stage. The damage size can be determined from the damage indicator value for a known damage scenario (as applied in the damage tolerance analysis), from finite element analyses, making it a level 3 SHM system. The presented damage indicator is not sensitive for temperature effects and therefore the SHM system does not require additional temperature sensors. Also, the damage indicator is not sensitive for the applied load time variation, making it robust, and it can be computed on a flight-by-flight basis, drastically reducing the inspection interval. Moreover, it can distinguish a debonded sensor from a load path failure and a broken fibre or sensor can easily be detected by the sensor system, preventing falls calls.

Acknowledgements

References

[1]   Military Specification, Airplane damage tolerance requirements, *MIL-A-83444 (USAF)*, 1987.

[2]   DeFazio M and Yeh H, Structures Bulletins EN-SB-08-001/002/003 on Fail-Safe structures, 2008 *http://www.saf-engineering.com/images/EN-SB-08-001.pdf*.

[3]   Hannan MA, Hassan Md Kamrul and Ker PJ, A review on sensors and systems in structural health monitoring: Current issues and challenges *Smart Struct. Syst.* 22(5) 509-525, 2018.

[4]   Udd E, An overview of fibre-optic sensors *Rev. Sci. Instrum.* 66 4015-4030, 1995.

[5]   Evenblij RS and Leijtens JAP, Space Gator: a giant leap for fibre optic sensing *ICSO*, 2014

    https://www.technobis.com/index.php/products/fiber-sensing-solutions/gator-basic-fbg-interrogator/.

[6]   High speed interrogator for acoustic emission, https://optics11.com/products/multizona.

[7]   Kwon H, Park Y, et al., Embedded fibre Bragg grating sensor–based wing load monitoring system for composite aircraft, Structural Health Monitoring, 18(4), pp 1337-1351, 2019.

[8]   Kirikera GR, Balogun O, Krishnaswamy S, Adaptive Fiber Bragg Grating Sensor Network for Structural Health Monitoring: Applications to Impact Monitoring, 10(1), pp 5-16, 2010.

[9]   Doebling SW, Farrar CR and Prime MB, A Summary Review of Vibration-based Damage Identification Methods, Structural Health Monitoring, 30, pp. 91-105, 1998.

[10] Montalvão D, Maia NMM and Ribeiro AMR, A Review of Vibration-based Structural Health Monitoring with Special Emphasis on Composite Materials, Structural Health Monitoring, 38(4), pp. 295-324, 2006.

[11] Li F and Kageyama K, Guided Wave and Damage Detection in Composite Laminates Using Different Fiber Optic Sensors. Sensors, 4005-4021, 2009.

[12] Tian Z, Yu L, et al., Damage localization with fibre Bragg grating Lamb wave sensing through adaptive phased array imaging, Structural Health Monitoring, 18(1), pp 334-344, 2018.

[13] Jonge de JB, Crack severity index of monitored load spectra *Int J Fatigue* 18(4) 274, 1996.

[14] Lee H, Park S and Kim H, Estimation of Aircraft Structural Fatigue Life Using the Crack Severity Index Methodology, J. of Aircraft, 47(5), 2010.

[15] Molent L and Forrester C, The lead crack concept applied to defect growth in aircraft composite structures *Comp. Struct.* 166 22–26, 2017.

[16] Tada H, Paris PC and Irwin GR, The stress analysis of cracks handbook, 1985.

NLR - Royal Netherlands Aerospace Centre

Royal NLR operates as an unaffiliated research centre, working with its partners towards a better world tomorrow. As part of that, Royal NLR offers innovative solutions and technical expertise, creating a strong competitive position for the commercial sector.

Royal NLR has been a centre of expertise for over a century now, with a deep-seated desire to keep innovating. It is an organisation that works to achieve sustainable, safe, efficient and effective aerospace operations.
The combination of in-depth insights into customers' needs, multidisciplinary expertise and state-of-the-art research facilities makes rapid innovation possible. Both domestically and abroad, Royal NLR plays a pivotal role between science, the commercial sector and governmental authorities, bridging the gap between fundamental research and practical applications. Additionally, Royal NLR is one of the large technological institutes (GTIs) that have been collaborating since 2010 in the Netherlands on applied research as part of the TO2 federation.

From its main offices in Amsterdam and Marknesse plus two satellite offices, Royal NLR helps to create a safe and sustainable society. It works with partners on numerous (defence) programmes, including work on complex composite structures for commercial aircraft and on goal-oriented use of the F-35 fighter. Additionally, Royal NLR helps to achieve both Dutch and European goals and climate objectives in line with the Luchtvaartnota (Aviation Policy Document), the European Green Deal and Flightpath 2050, and by participating in programs such as Clean Sky and SESAR.

For more information visit: **www.nlr.org**